GSK2801, a BAZ2/BRD9 Bromodomain Inhibitor, Synergizes with BET Inhibitors to Induce Apoptosis in Triple-Negative Breast Cancer

Samantha M. Bevill[1], Jose F. Olivares-Quintero[1], Noah Sciaky[1], Brian T. Golitz[1], Darshan Singh[1], Adriana S. Beltran[1], Naim U. Rashid[2], Timothy J. Stuhlmiller[1], Andrew Hale[3], Nathaniel J. Moorman[3], Charlene M. Santos[4], Steven P. Angus[1], Jon S. Zawistowski[1], and Gary L. Johnson[1]

Abstract

Screening of an inhibitor library targeting kinases and epigenetic regulators identified several molecules having antiproliferative synergy with extraterminal domain (BET) bromodomain (BD) inhibitors (JQ1, OTX015) in triple-negative breast cancer (TNBC). GSK2801, an inhibitor of BAZ2A/B BDs, of the imitation switch chromatin remodeling complexes, and BRD9, of the SWI/SNF complex, demonstrated synergy independent of BRD4 control of P-TEFb–mediated pause-release of RNA polymerase II. GSK2801 or RNAi knockdown of BAZ2A/B with JQ1 selectively displaced BRD2 at promoters/enhancers of ETS-regulated genes. Additional displacement of BRD2 from rDNA in the nucleolus coincided with decreased 45S rRNA, revealing a function of BRD2 in regulating RNA polymerase I transcription. In 2D cultures, enhanced displacement of BRD2 from chromatin by combination drug treatment induced senescence. In spheroid cultures, combination treatment induced cleaved caspase-3 and cleaved PARP characteristic of apoptosis in tumor cells. Thus, GSK2801 blocks BRD2-driven transcription in combination with BET inhibitor and induces apoptosis of TNBC.

Implications: Synergistic inhibition of BDs encoded in BAZ2A/B, BRD9, and BET proteins induces apoptosis of TNBC by a combinatorial suppression of ribosomal DNA transcription and ETS-regulated genes.

Introduction

Inhibitors of the bromodomain (BD) and extraterminal domain (BET) epigenetic readers have shown preclinical promise in multiple types of cancer, notably in acute myelogenous leukemia (AML) where BET proteins play a critical role in maintaining transcription of *MYC* (1–3). BRD2/3/4 interact with acetyl-lysine residues on histone tails and nonhistone proteins via their BDs. Their regulatory function is, in part, attributed to the ability of BRD4 to associate with and recruit the positive transcription elongation factor (P-TEFb) complex via interactions involving its unique C-terminal domain (CTD). P-TEFb is a multisubunit complex composed of CDK9 and its regulatory subunit cyclin T1. P-TEFb promotes productive gene transcription in concert with additional transcriptional coactivators (Mediator complex) and chromatin-modifying enzymes [CREB-binding protein (CBP)/p300]. BRD4 is the best characterized BET family member, which recruits and activates the P-TEFb complex leading to transcriptional elongation through CDK9-catalyzed phosphorylation of serine 2 in the CTD of RNA polymerase II (Pol II; refs. 4, 5).

In addition to inhibition of tumor growth as single agents, BET BD inhibitors (BETi) have been shown to block adaptive resistance in combination with inhibitors targeting receptor tyrosine kinases and the MEK–ERK and PI3K pathways (6–9). Inhibition of these signaling networks results in genome-wide enhancer formation involving the seeding of BRD4, MED1, H3K27 acetylation, and CBP/p300 that drives P-TEFb–dependent transcriptional adaptation (6). BETi blocks enhancer remodeling and prevents P-TEFb–dependent transcriptional adaptive reprogramming, making the action of the kinase inhibitors more durable and actually preventing or reversing resistance (6).

Preclinical models of breast cancer are generally sensitive to inhibition of BET BD-dependent transcription (7, 10, 11), specifically triple-negative breast cancer (TNBC; ref. 12), which is a heterogeneous and aggressive disease defined by the absence of targetable receptors for estrogen and progesterone, and HER2 (13, 14). Clinical trials are currently testing the efficacy of BETi in treating TNBC, other solid tumors, and hematologic malignancies (ClinicalTrials.gov). Both BRD2 and BRD4 are

[1]Department of Pharmacology, Lineberger Comprehensive Cancer Center, University of North Carolina School of Medicine, Chapel Hill, North Carolina.

[2]Department of Biostatistics, Lineberger Comprehensive Cancer Center, University of North Carolina School of Medicine, Chapel Hill, North Carolina.

[3]Department of Microbiology and Immunology, Lineberger Comprehensive Cancer Center, University of North Carolina School of Medicine, Chapel Hill, North Carolina. [4]Department of Genetics, Lineberger Comprehensive Cancer Center, University of North Carolina School of Medicine, Chapel Hill, North Carolina.

Note: Supplementary data for this article are available at Molecular Cancer Research Online (http://mcr.aacrjournals.org/).

Corresponding Author: Gary L. Johnson, University of North Carolina at Chapel Hill, 4079 Genetic Medicine Building, 120 Mason Farm Road, Chapel Hill, NC 27599. Phone: 919-843-3106; Fax: 919-966-5640; E-mail: glj@med.unc.edu

overexpressed in basal-like TNBC, but the functional distinctions in the mechanisms by which BRD2 and BRD4 regulate transcription independent of P-TEFb activation remain poorly defined.

We performed dose-dependent drug synergy screens against inhibitors targeting the BET BD to define novel combinatorial strategies that selectively enhanced growth inhibition by BETi in TNBC. Of particular interest was the novel drug synergy we discovered between inhibitors targeting additional families of BDs encoded in CBP/p300, BAZ2A/B, and BRD9. GSK2801, an inhibitor of the BDs of BAZ2A (TIP5), BAZ2B, and BRD9 (BD-containing protein 9) showed little or no growth inhibition as a single agent, yet combined treatment with BETi resulted in strong growth inhibition of TNBC. BRD9, whose BD binds GSK2801 with a lower affinity than the BD of BAZ2A/B, is a member of the SWI/SNF regulatory complex that regulates chromatin remodeling and transcription. Bromodomain adjacent to zinc finger domain (BAZ2) proteins function as regulatory subunits that pair with one of two ATPases, SMARCA1 (SNF2L) or SMARCA5 (SNF2H), to form the core of imitation switch chromatin remodeling complexes (ISWI; ref. 15). BAZ2A binds SMARCA5 to form the nucleolar remodeling complex (NoRC), which maintains a pool of heterochromatic ribosomal DNA (rDNA; ref. 16). NoRC function is important not only to temper the amount of rDNA copies accessible for transcription, of which there are hundreds in a given mammalian cell, but also to maintain genomic stability of these highly repetitive regions. This protective function of the NoRC also extends to centromeres and telomeres (17, 18). Little is known about the function of BAZ2B; it was recently reported that BAZ2B forms stable complexes with both ATPases making it a novel ISWI regulatory subunit (19).

The TCGA pan-cancer dataset indicates BAZ2A and BAZ2B are not frequently mutated across cancer with the exception of uterine corpus endometrial carcinoma where both BAZ2A and BAZ2B are mutated in greater than 10% of tumors. Increased expression of BAZ2A/B mRNA is observed across several tumor types including thyroid carcinoma and AML. A superenhancer enriched for H3K27Ac was recently identified proximal to the *BAZ2B* gene in AML (20). BAZ2B is consistently highly expressed in AML with no change in copy number, suggesting epigenetic mechanisms of BAZ2A/B overexpression. BRD9 is also not frequently mutated in the TCGA pan-cancer dataset but is significantly amplified in lung cancers. BRD9 has also been implicated in driving AML growth as a subunit of the SWI/SNF complex via regulation of *MYC* transcription (21).

Our screening results provide a series of synergistic drug combinations to achieve durable inhibition of TNBC cell proliferation with BET or CBP/p300 BD inhibitors. These data highlight a unique mechanism of synergy between the BAZ2/BRD9 BD inhibitor GSK2801 and BETi. Drug synergy was not observed between GSK2801 and other inhibitors of P-TEFb transcriptional activation including CBP/p300 and CDK9 inhibitors, indicating a mechanism of synergy unrelated to pause-release of Pol II. Instead, loss of BRD2 from chromatin following combined GSK2801 and BETi blocked ETS-regulated gene transcription in the nucleoplasm as well as nucleolar transcription of rRNA. These findings support distinct functional roles of BRD2 in regulating nucleoplasmic and nucleolar transcription relative to other BET family proteins. Furthermore, these results reveal unique adaptive mechanisms of BRD2 on chromatin in response to BETi, which are amenable to coinhibition of BAZ2/BRD9 BDs to induce apoptosis in 3D-spheroid cultures of TNBC.

Materials and Methods

Cell culture

HCC1806, WHIM12, and MDA-MB-468 cells were maintained in RPMI1640 medium (Gibco, Thermo Fisher Scientific) supplemented with 10% FBS, 1,000 U/mL Penicillin and 1 mg/mL Streptomycin. MDA-MB-231 and SUM-159 cells were maintained in DMEM/F12 1:1 medium (Gibco, Thermo Fisher Scientific) supplemented with 5% FBS, 5 μg/mL insulin, 1 μg/mL hydrocortisone, 1,000 U/mL penicillin, and 1 mg/mL streptomycin. SUM-149(+) and WHIM2 cells were maintained in HuMEC medium with defined media supplements (Gibco, Thermo Fisher Scientific) and supplemented with 5% FBS, 1,000 U/mL penicillin, and 1 mg/mL streptomycin. SUM-149(+) cells used in this study contain EpCAM$^+$/CD45f$^+$ cells, which were isolated via FACS from the heterogeneous parental SUM-149 cell line.

Cell line authentication

All cell lines were obtained from the Lineberger Comprehensive Cancer Center as well as collaborating labs. Whim2 and Whim12 cell lines derived from PDXs have been whole-exome sequenced and RNA-sequenced for reference. All other cell lines used in this study have been authenticated by the Johns Hopkins Genetics Core Resources Facility using their short-tandem repeat testing. Cell lines are annually tested in the lab for *Mycoplasma*. Cell lines were passaged no longer than one month for all experiments performed.

Compounds

Information on compounds used in screening and subsequent validation experiments is listed in Supplementary Data File 1. BI-9564 (catalog. no. S8113) was obtained from Selleckchem and BAZ2-ICR (catalog. no. SML1276) was obtained from Sigma-Aldrich.

Synergy screening

The optimal dose range for JQ1, OTX015, or CPI-637 was determined for each cell line screened across half-log doses. JQ1 and OTX015 screens were performed in 6 × 6 dose-response matrices. MDA-MB-231, SUM-149(+), and WHIM12 cell lines were treated with 3 nmol/L–1 μmol/L JQ1. HCC1806, WHIM2, and MDA-MB-468 cell lines were treated with 10 nmol/L–3 μmol/L JQ1. MDA-MB-231 cells were dosed with 10 nmol/L–3 μmol/L OTX015. All CPI-637 screens were performed in 5 × 6 dose-response matrices. MDA-MB-231, HCC1806, WHIM2, and WHIM12 cells were dosed with 100 nmol/L–10 μmol/L CPI-637 in half-log doses. Cells were seeded in 384-well plates using a BioTek microplate dispenser. The following day cells were dosed with drug using a Beckman Coulter Biomek FX instrument. The screening library was tested for growth inhibition alone or in combination across 6 doses of the screening library: 10 nmol/L, 100 nmol/L, 300 nmol/L, 1 μmol/L, 3 μmol/L, and 10 μmol/L. Bortezomib (1 μmol/L) was included as a positive control or 0.1% DMSO as a negative control for growth inhibition on each plate. Plates were incubated at 37°C for 96 hours and lysed by adding 10-μL CellTiter-Glo Reagent (Promega, catalog. no. G7570) to 50-μL cell media. Luminescence was measured using a PHERAstar FS instrument and growth inhibition was calculated relative to DMSO-treated wells.

Drug synergy analysis

Drug synergy scores were generated using the SynergyFinder package 1.6.1 (22). Bliss, Loewe, highest single agent (HSA), and zero interaction potency (ZIP) scores were calculated without baseline correction and using default parameters with the exception that Emin was specified as 0 and Emax as 100. Synergy was assessed across individual doses of each library compound to generate six possible scores per compound. To be considered a hit, a given compound had to generate a positive mean synergy score for at least 1 dose tested in 5 of 6 (for JQ1 screening data) or 3 of 4 (for CPI-637 screening data) cell lines screened. Hits were then ranked by the mean of all synergy scores produced in the drug combination matrix. Synergy scores represent the percent growth inhibition induced by a drug combination, which exceeded the expected growth inhibition. Expected growth inhibition was calculated on the basis of the effect of each drug as a single agent.

Chromatin immunoprecipitation and library preparation

Chromatin immunoprecipitation (ChIP) experiments were performed as described in (6). Briefly, approximately 1×10^7 cells per immunoprecipitation were cross-linked 10 minutes at room temperature in 1.1% formaldehyde. Nuclear extracts were sonicated 15 cycles (30-second pulse, 30-second cooling) using a Bioruptor Pico (Diagenode). Samples were tumbled overnight at 4°C with 10-μg antibody conjugated to protein A Dynabeads (Thermo Fisher Scientific). Following reverse cross-linking and RNase/proteinase K treatment, DNA was eluted from beads and purified using Qiagen MinElute PCR purification columns. Chromatin immunoprecipitation coupled with deep sequencing (ChIP-seq) libraries were prepared using the KAPA HyperPrep Kit according to the manufacturer's instructions. For each set of experimental samples an equal amount of DNA was used to generate libraries (between 10–50 ng depending on experiment). Samples were indexed using Illumina TruSeq indexed adapters. Dual size selection was performed following 12–18 cycles PCR amplification. Samples were 12-plexed and single-end 75 bp reads were generated using an Illumina NextSeq-500. Raw and processed ChIP-seq datasets have been uploaded to GEO (accession no. GSE116919).

RNA-sequencing

Four microgram of total RNA was isolated from cells using the Qiagen RNeasy Plus Kit. Sequencing libraries were prepared using the KAPA stranded mRNA-seq kit according to the manufacturer's instructions with the exception that libraries were amplified 10 cycles by PCR. Samples were indexed using Illumina TruSeq indexed adapters. Samples were 12-plexed and run on an Illumina NextSeq-500 to produce 75-cycle single-end reads.

RNA-sequencing analysis

RNA-seq datasets of TNBC patient tumors and cell lines used in Fig. 1C and D are deposited in dbGaP (phs001405.v1.p1) and GEO (accession no. GSE87424), respectively. Data was generated and processed as cited in (6). Briefly datasets were aligned to the human reference genome (hg19_M_rCRS) using MapSplice (23), sorted and indexed using SAMtools v1.2 (24), and transcript abundance estimates were generated using the RSEM expectation-maximization algorithm (25).

For drug-treated datasets used in the rest of the manuscript, QC-passed reads were aligned to the human reference genome (hg38) using STAR 2.4.2a (26) and reads were translated to transcriptome coordinates using Salmon 0.60 (27). Isoform data were collated to single-gene IDs using the R package biomaRt (28), and abundance estimates were upper quartile normalized using R. Raw and processed RNA sequencing (RNA-seq) data have been uploaded to GEO (accession no. GSE116919).

Gene set enrichment analysis

Gene set enrichment analysis (GSEA) was run on drug-treated RNA-seq datasets according to instructions at http://software. broadinstitute.org/gsea/index.jsp. All Hallmark, GO, and Oncogenic Signature gene sets were analyzed using the following parameters: number of permutations, 1,000; permutation type, gene_set; enrichment statistic, weighted; metric for ranking genes, Signal2Noise; gene set maximum size, 500; gene set minimum size, 15.

ChIP-seq analysis

ChIP-seq datasets were aligned using Bowtie v1.1.2 (29) to the human reference genome (hg19) or to a single copy of the ribosomal DNA repeat (GenBank: U13369.1). Alignments were performed using the following parameters: -v 2 – m 1. All analysis was performed using RefSeq (30) hg19 human gene annotations. Read density was normalized to the total number of million mapped reads (rpm). Data was normalized by subtracting read density of the input chromatin from the ChIP read density. HCC1806 and SUM-159 input datasets were used from (6), GEO accession no. GSE87424. MACS 2.2.2.20160309 (31) and HMCan v1.28 (32) were used to call enriched regions. We found that MACS was not calling peaks in the regions with high copy-number variation and therefore used HMCan to call peaks in these regions. MACS was run using default settings. HMCan was run with narrow peak calling configuration file with no blacklisted regions. Peaks within 12.5 kb of each other were stitched as described previously (33). For comparative analysis across drug treatments, union peaks were defined, which represent a collection of peak regions across all the treatment datasets in a project. Peak classification was performed as described in (6) and python code generated in the laboratory for ChIP-seq analysis is available at https://github.com/darshansinghunc/chippeakanalysis.
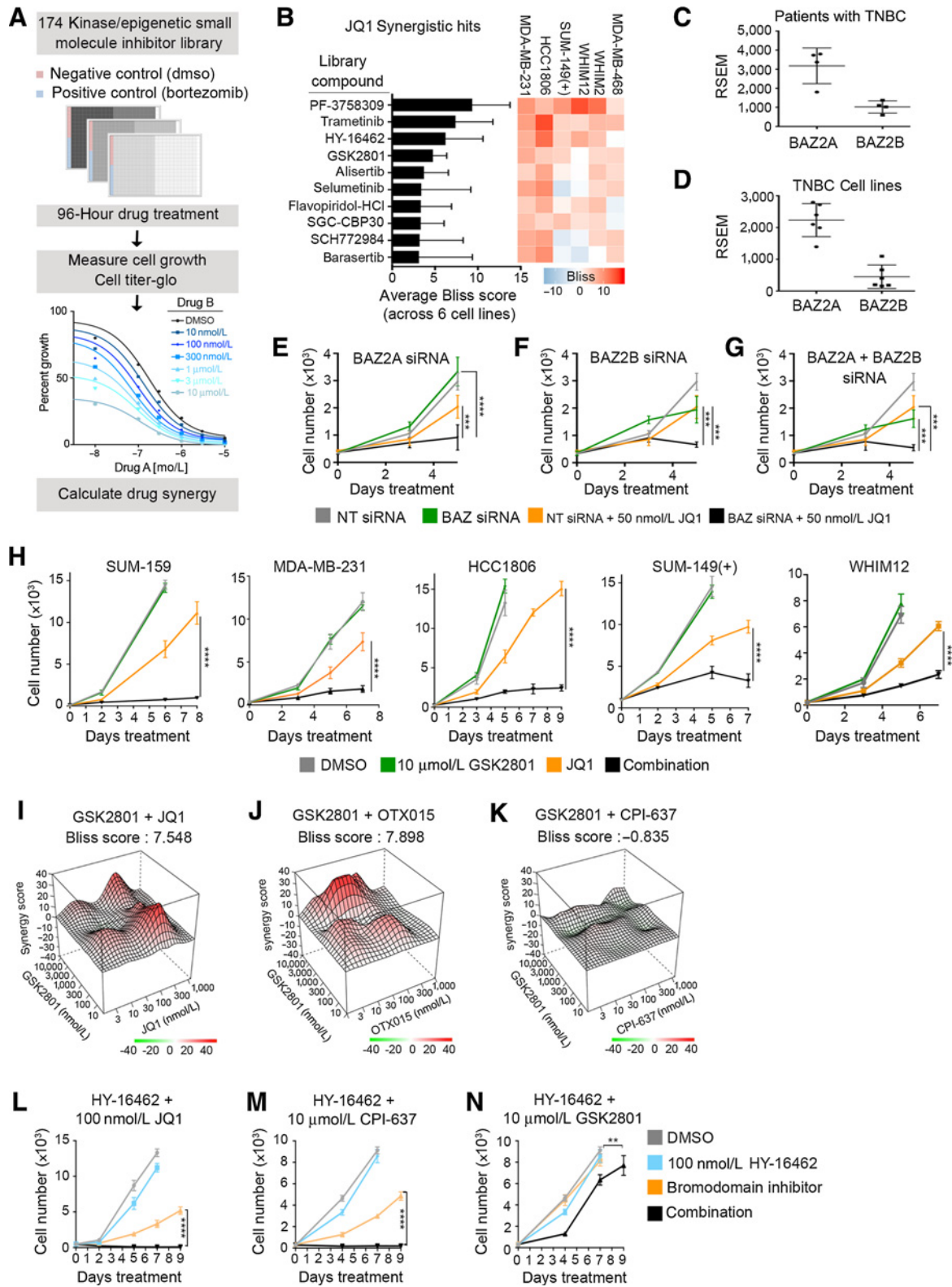
A peak in dataset A was considered overlapped by dataset B if 40% of the length of the peak in dataset A was covered by a peak in dataset B.

ChIP-seq data visualization. For ribosomal DNA alignments, reads were normalized to the total number of reads mapped to the hg19 reference genome per sample. Read counts were recorded in 250 bp bins and data were plotted using R. For fold change plots a floor of 5 rpm was created to avoid artificially high fold change values.

ChIP-seq density tracks in Fig. 3L–O and Supplementary Fig. S4F and S4G were created by normalizing data to the total number of mapped reads. Read counts were plotted using Python.

Box-and-whisker plots for ChIP-seq datasets were generated using peaks with greater than or equal to 5 rpm density in, at least, one treatment condition. Paired *t* tests were performed to measure statistical differences between samples.

All metagene plots and heatmaps were generated using HOMER (34). A total of 25 bp bins were used to generate all

A 174 Kinase/epigenetic small molecule inhibitor library

Negative control (dmso)
Positive control (bortezomib)

↓

96-Hour drug treatment

↓

Measure cell growth
Cell titer-glo

↓

Drug B
DMSO
10 nmol/L
100 nmol/L
300 nmol/L
1 µmol/L
3 µmol/L
10 µmol/L

Percent growth vs Drug A [mol/L]

↓

Calculate drug synergy

B JQ1 Synergistic hits

Library compound:
PF-3758309
Trametinib
HY-16462
GSK2801
Alisertib
Selumetinib
Flavopiridol-HCl
SGC-CBP30
SCH772984
Barasertib

Average Bliss score (across 6 cell lines)

Cell lines: MDA-MB-231, HCC1806, SUM-149(+), WHIM12, WHIM2, MDA-MB-468

Bliss: −10   0   10

C Patients with TNBC
RSEM — BAZ2A, BAZ2B

D TNBC Cell lines
RSEM — BAZ2A, BAZ2B

E BAZ2A siRNA
Cell number (×10³) vs Days treatment

F BAZ2B siRNA
Cell number (×10³) vs Days treatment

G BAZ2A + BAZ2B siRNA
Cell number (×10³) vs Days treatment

NT siRNA | BAZ siRNA | NT siRNA + 50 nmol/L JQ1 | BAZ siRNA + 50 nmol/L JQ1

H SUM-159 | MDA-MB-231 | HCC1806 | SUM-149(+) | WHIM12
Cell number (×10³) vs Days treatment

DMSO | 10 µmol/L GSK2801 | JQ1 | Combination

I GSK2801 + JQ1
Bliss score : 7.548
Synergy score — GSK2801 (nmol/L), JQ1 (nmol/L)
−40 −20 0 20 40

J GSK2801 + OTX015
Bliss score : 7.898
synergy score — GSK2801 (nmol/L), OTX015 (nmol/L)
−40 −20 0 20 40

K GSK2801 + CPI-637
Bliss score : −0.835
synergy score — GSK2801 (nmol/L), CPI-637 (nmol/L)
−40 −20 0 20 40

L HY-16462 + 100 nmol/L JQ1
Cell number (×10³) vs Days treatment

M HY-16462 + 10 µmol/L CPI-637
Cell number (×10³) vs Days treatment

N HY-16462 + 10 µmol/L GSK2801
Cell number (×10³) vs Days treatment

DMSO | 100 nmol/L HY-16462 | Bromodomain inhibitor | Combination

plots surrounding ± 2 kb of the annotated tss or peak center. Heatmaps were visualized using Java Treeview (35).

Motif enrichment analysis. HOMER was employed to define motifs enriched at BRD2-occupied genomic loci. All BRD2 peaks greater than or equal to 5 rpm in DMSO control samples were used for each cell line analyzed. Default parameters were used to search a 200 bp window surrounding peak centers.

Tumor spheroids

Tumor cells expressing red fluorescent protein (RFP) were plated in low-adhesion round-bottom 96-well plates as monocultures or were cocultured with reduction mammoplasty fibroblasts (RMF) expressing GFP. For SUM-149(+) spheroids, 5,000 tumor cells were seeded per well or mixed at a 1:1 ratio with RMFs. For WHIM12 spheroids, 1,000 tumor cells were mixed with 2,000 RMFs per well. Spheroids were given 48 hours to form before beginning drug treatment. At endpoint, cell fluorescence was imaged using an Evos FL Auto 2 instrument. Following imaging, spheroids were lysed in CellTiter-Glo 3D (Promega, catalog. no. G9681) by adding 50-µL reagent to 150-µL cell media. Plates were rotated at 150 rpm for 30 minutes before luminescence was read using a PHERAstar FS.

Results

High-throughput identification of synergistic drug combinations with BETi in TNBC

A 175 compound, small-molecule inhibitor library targeting protein kinases and epigenetic modifiers was used in 6×6 dose-response matrices to screen for drug synergy in combination with BD inhibitors (Fig. 1A). Library compounds were selected on the basis of target diversity, as well as indication of clinical success, and suitable FDA-approval (Supplementary Data File 1). We screened six TNBC cell lines representing TNBC basal-like and claudin-low molecular subtypes (36, 37) against JQ1, a BETi. The cell lines displayed a range of baseline sensitivities to JQ1 (IC$_{50}$s ranged from 37.4 nmol/L to 1.1 µmol/L; Supplementary Fig. S1A). Synergy was assessed using multiple computational models (22) including HSA, the Loewe additivity model (Loewe), the Bliss independence model (Bliss), and the ZIP (Supplementary Data File 2; ref.38). Common hits identified in all cell lines across all synergy models (Fig. 1B; Supplementary Fig. S1B) were validated with an additional BETi, OTX015 (39), in the MDA-MB-231 cell line (Supplementary Data File 3).

Inhibition of previously identified targets: MEK1/2-ERK1/2 [trametinib and selumetinib (MEKi), SCH772984 (ERKi)], P-TEFb [HY-16462 and flavopiridol (CDK9i), SGC-CBP30 (CBP/p300i; ref 6)], and Aurora kinase (alisertib and barasertib; ref. 11), validated the synergy screen (Fig. 1B; Supplementary Fig. S1C–S1F). Among the other top hits was PF-3758309 that selectively targets PAK4 with higher potency than other PAK family members. PF-3758309 caused cell shape changes and diminished adherence in 2D culture of multiple TNBC cell lines. Western blots showed no reduction in pERK1/2 or pAKT following combination PAK/BET BD inhibition (Supplementary Fig. S1G), suggesting loss of cell number in 2D screens was due to cytoskeletal changes. PF-3758309 was not further pursued because clinical trials for this compound have been terminated and other PAKi have not progressed in patient trials despite significant numbers of studies in preclinical models (ClinicalTrials.gov).

Of particular interest from the screen hits was the novel drug synergy observed between BETi and GSK2801, an inhibitor of BAZ2A and BAZ2B BDs with partial activity against the BRD9 BD. BAZ2A and BAZ2B are members of the BD adjacent to zinc finger domain (BAZ) protein family and contain a PHD domain and homologous BD (40). We observed similar expression levels by RNA-seq of BAZ2A and BAZ2B between primary TNBC patient tumors (dbGaP: phs001405.v1.p1) and cell lines (Fig. 1C and D). BAZ2A is expressed more highly than BAZ2B in TNBC cell lines at an average RSEM read count of 2,233 compared with 451, respectively. Knockdown via RNAi of BAZ2A and B in combination with JQ1 resulted in significant growth inhibition (Fig. 1E–G; Supplementary Fig. S1H), consistent with the screening results. We further validated synergistic growth inhibition with combination GSK2801 and JQ1 in a panel of TNBC cell lines (Fig. 1H).

In addition to binding the BDs of BAZ2A/B, GSK2801 has reported binding activity for the BD of BRD9 (41), a member of the SWI/SNF chromatin remodeling complex. AlphaScreen assays confirmed GSK2801 interacted with the BRD9 BD. In contrast, a second BAZ2A/B inhibitor, BAZ2-ICR (42), showed no interaction with the BRD9 BD (Supplementary Fig. S2A–S2C). Neither inhibitor displayed activity against the BET BD (Supplementary Fig. S2D). Dose-dependent growth curves revealed that 3 µmol/L GSK2801, which inhibits BAZ2A/B BDs but not the BRD9 BD, produced partial growth suppression in combination with JQ1 compared with 10 µmol/L GSK2801 (Supplementary Fig. S2E). Using RNAi targeting BRD9 in combination with JQ1 produced enhanced growth suppression (Supplementary Fig. S2F and S2G). Thus, inhibition of BRD9 by GSK2801 contributed to growth

Figure 1.
Drug synergy screens against BET and p300 BD inhibitors in TNBC cell lines. **A,** Schematic for screening approach. Cells were plated in 384-well plates and treated 96 hours with 6×6 dose concentrations of library compound in combination with either JQ1 (BETi) or CPI-637 (p300i). Cell viability was measured with CellTiter-Glo and drug synergy was quantified using Synergy Finder. **B,** Drug synergy rankings using Bliss scoring for JQ1 screens (performed in MDA-MB-231, HCC1806, SUM-149(+), MDA-MB-468, WHIM2, and WHIM12). Synergy scores represent the percent inhibition observed following combination treatment, which exceeded the expected growth inhibition as calculated by the Bliss independence model. Values were generated by first calculating the mean Bliss score across the full drug synergy matrix for each cell line (36 possible dose combinations). **C** and **D,** RNA-seq reads of BAZ2A and BAZ2B expression in primary TNBC patient samples (**C**) versus 6 TNBC cell lines (**D**) used for screening. **E–G,** MDA-MB-231 growth curves transfected with nontargeting (NT) or BAZ2 siRNAs in combination with 50 nmol/L JQ1. Error bars, ± SD, $n = 6$. P values were calculated using two-tailed t tests. **H,** Growth curves across multiple TNBC cell lines with 10 µmol/L GSK2801. JQ1 doses were determined on the basis of the relative sensitivity of each cell line. MDA-MB-231: 30 nmol/L JQ1, SUM159: 100 nmol/L JQ1, SUM-149(+) and WHIM12: 300 nmol/L JQ1, HCC1806: 500 nmol/L JQ1. Error bars, ± SD, $n = 6$. P values comparing JQ1 versus combination drug treatment were calculated using two-tailed t tests. **I–K,** 3D drug interaction landscapes produced using SynergyFinder between GSK2801 and JQ1/OTX015 or CPI-637 in the MDA-MB-231 cell line following 96-hour drug treatment. **L–N,** MDA-MB-231 growth curves with 100 nmol/L HY-16462 in combination with 100 nmol/L JQ1, 10 µmol/L CPI-637, or 10 µmol/L GSK2801. Error bars, ± SD, $n = 6$. P values comparing BDi versus combination drug treatment were calculated using two-tailed t tests.

inhibition observed with combination drug treatment (JQ1 + GSK2801). Combining the selective BAZ2 BD inhibitor BAZ2-ICR with the selective BRD9 inhibitor BI-9564 elicited complete growth suppression in combination with JQ1, as seen with GSK2801 and JQ1 (Supplementary Fig. S2H). Western blots showed a BRD9-dependent reduction of c-MYC levels relative to JQ1 alone (Supplementary Fig. S2I), consistent with the role of BRD9 maintaining *MYC* expression and rapid cell proliferation as a member of the SWI/SNF complex (21).

Synergy screens were also performed with CPI-637, an inhibitor of the CBP/p300 BD, to assess the overlap of therapeutic vulnerabilities to those found with BETi (Supplementary Data File 4). Reports of the significant activity of kinase inhibitors on BET BDs (43–45) led us to perform AlphaScreen assays across four doses (10 nmol/L, 100 nmol/L, 1 µmol/L, and 10 µmol/L) of our screening library to control for binding against the BET and CBP/p300 BDs (Supplementary Data File 5). None of the screen hits displayed off-target activity at previously defined synergistic doses against either the BET or CBP/p300 BD (Supplementary Fig. S2J), which might otherwise account for drug synergy. We observed significant overlap between the BETi and CBP/p300i screening datasets, suggesting BET protein function is tightly linked to CBP/p300 acetyltransferase activity (Supplementary Fig. S2K). Uniquely, GSK2801 only displayed growth inhibition in combination with BETi, JQ1, and OTX015, and not the CBP/p300i CPI-637 (Fig. 1I–K). Furthermore, GSK2801 did not synergize with inhibition of CDK9, another member of the P-TEFb complex, compared with p300i and BETi (Fig. 1L–N). This indicates a mechanism of synergy between GSK2801 and BETi, which is independent of P-TEFb–mediated transcriptional activation controlled by BRD4.

Selective BRD2, 4 and 9 displacement from chromatin following treatment with BETi (JQ1), and BAZ2A/B BD inhibitor (GSK2801)

To gain a more comprehensive understanding of how BD proteins respond to GSK2801 and JQ1 treatment, we quantified BRD2, BRD4, and BRD9 on chromatin via ChIP-seq. Both BRD2 and BRD4, whose BDs bind JQ1, were significantly lost from chromatin following single-agent JQ1 treatment (Fig. 2A and B). There is a large degree of overlap between BET proteins at baseline with 38% of BRD4 peaks overlapping with BRD2 and almost all BRD2 peaks (94%) overlapping with BRD4 peaks. Despite this cooccupancy of chromatin peaks, relative to JQ1 treatment alone, only BRD2 but not BRD4 showed an enhanced loss from chromatin with JQ1 + GSK2801 combination drug treatment (Fig. 2A and B). Classification of BRD2 peaks showed GSK2801-dependent loss of BRD2 at both promoter and enhancer regions across the genome (Supplementary Fig. S3A and S3B). This indicates the interaction of GSK2801 with BAZ2A/B and BRD9 BDs causes dissociation of BRD2 but not BRD4 from chromatin in the context of JQ1 treatment.

ChIP-seq also was used to determine cooccupancy on chromatin between BRD9 and BET proteins. We observed overlap between BRD4 and BRD9 independent of BRD2, but overlap between BRD2 and BRD9 was only observed when BRD4 was also present (Supplementary Fig. S3C). This suggests BRD9 is in chromatin complexes that include BET proteins, most notably BRD4. BRD9 was lost from chromatin following BETi despite the specificity of JQ1 for BET BDs and not the BRD9 BD (Fig. 2C). We

did not observe enhanced loss of BRD9 from chromatin following the addition of BAZ2i to the JQ1 treatment. This contrasts with BRD2, whose dissociation from chromatin is greater with the combination of GSK2801 + JQ1 than seen with JQ1 alone (Fig. 2B and C).

We observed a modest, but significant, increase in binding of BET proteins and BRD9 to chromatin across our ChIP experiments with single-agent GSK2801 treatment (Fig. 2A–C). The majority of these peaks were classified at promoter regions and did not correlate with regions most responsive to JQ1 treatment. BAZ2A, BAZ2B, and BRD9 are members of chromatin remodeling complexes and therefore, inhibition of their BDs may affect accessibility of chromatin and result in the increased chromatin occupancy of BRD2 and BRD9 that we observed following single-agent GSK2801 treatment.

ChIP-seq in an additional TNBC cell line, SUM-159, also showed significant loss of BRD2 from chromatin following combination treatment (GSK2801 + JQ1) relative to JQ1 alone (Supplementary Fig. S3D), consistent with BAZ2A/B proteins having a selective regulation of BRD2 relative to BRD4 and BRD9. Importantly, knockdown of either BAZ2A or BAZ2B phenocopied treatment with GSK2801 in combination with JQ1, with greater displacement measured by ChIP-seq of BRD2 relative to JQ1 treatment alone (Fig. 2D and E). Loss of BRD2 chromatin occupancy following combination BAZ2B RNAi/JQ1 treatment relative to JQ1 alone was confirmed in the HCC1806 cell line (Fig. 2F; Supplementary Fig. S3E).

Growth regulation in response to BRD2, BRD3, or BRD4 knockdown by siRNA

Knockdown of BET family proteins via RNAi in MDA-MB-231 cells revealed loss of BRD2 expression alone had little effect on growth, but induced strong growth inhibition in combination with GSK2801 (Fig. 2G). BRD3 loss of expression had no effect on growth in the presence or absence of GSK2801 (Fig. 2H). BRD4 knockdown caused a partial growth arrest alone and the addition of GSK2801 modestly enhanced growth arrest (Fig. 2I). In an additional cell line, SUM-149(+), we observed a significant growth inhibition with BRD2 knockdown alone and complete growth inhibition following the addition of GSK2801 (Supplementary Fig. S3F). We confirmed combined growth regulation between BRD2 and each BAZ protein via RNAi knockdown. Coknockdown of BRD2 and BAZ2A or BAZ2B enhanced growth inhibition of TNBC, with strong growth inhibition observed when all three proteins were lost (Fig. 2J–L), confirming inhibition of both BAZ2A and BAZ2B contribute to drug synergy with BETi. The strong growth inhibition observed with RNAi knockdown of BAZ2A/B contrasts with the partial growth inhibition observed using a selective BAZ2A/B BD inhibitor, BAZ2-ICR, in combination with JQ1 (Supplementary Fig. S2H). The reason for this is unclear, except for the difference between loss of the protein by knockdown versus the small-molecule BD inhibition of BAZ2A/B in the absence of BRD9 BD inhibition. Consistent with our screening data, knockdown of BRD2 did not enhance the antiproliferative effect of an inhibitor targeting the BD of CBP/p300 (SGC-CBP30) and a CDK9 inhibitor (HY-16462) in MDA-MB-231 cells (Supplementary Fig. S3G–S3I). Cumulatively, the findings demonstrate that BRD2, BAZ2A/B, and BRD9 control a chromatin network regulating cell growth independent of P-TEFb.
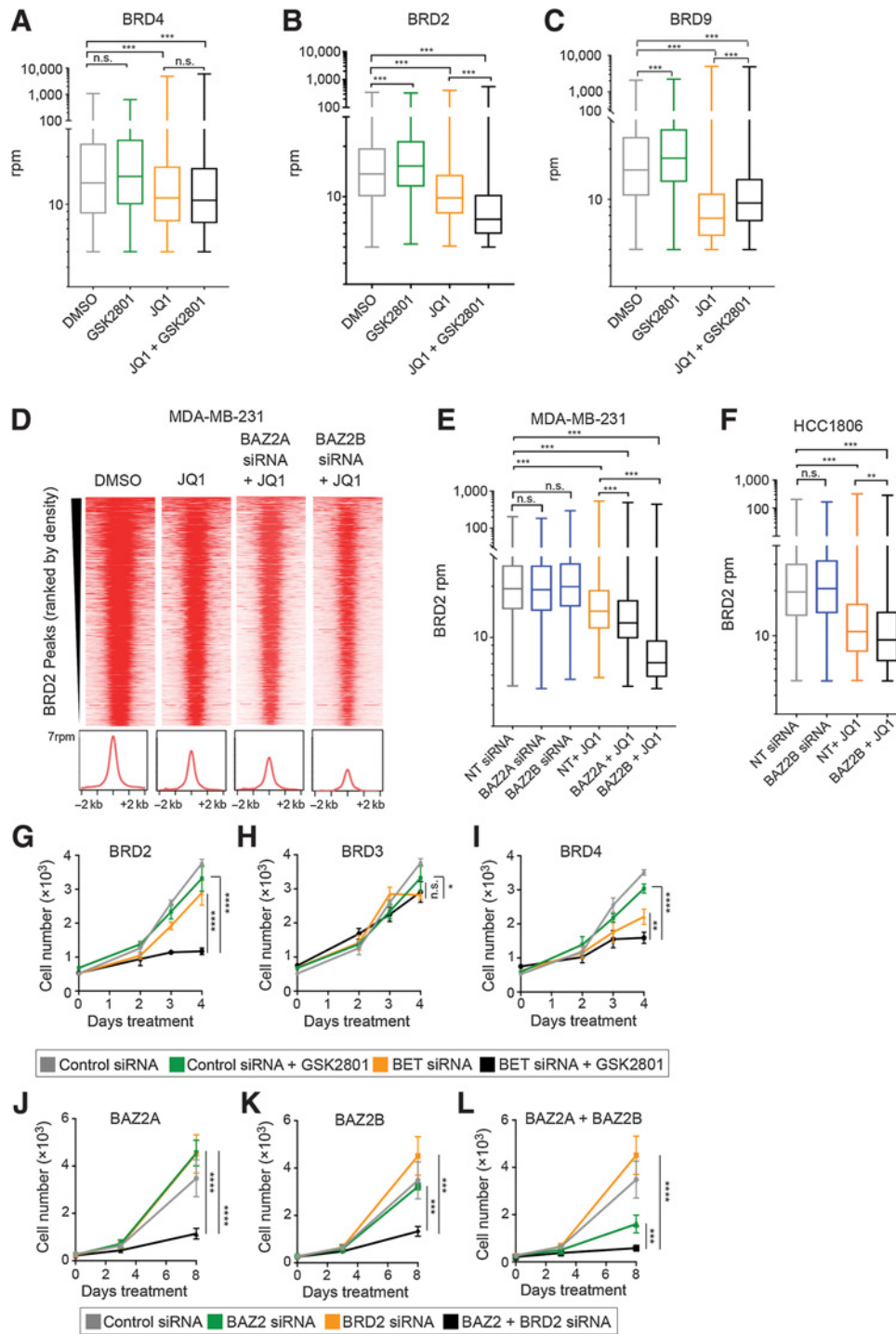
Figure 2.
BRD2 is displaced from chromatin following combination drug treatment. **A–C,** Levels of mapped BRD4 (**A**), BRD2 (**B**), and BRD9 (**C**) union peak density following 48-hour treatment with 100 nmol/L JQ1, 10 μmol/L GSK2801, or the combination in MDA-MB-231 cells. Statistical significance was measured via two-tailed, paired t tests. **D** and **E,** BRD2 peak density following transfection with 25 nmol/L nontargeting (NT), BAZ2A, or BAZ2B siRNA. MDA-MB-231 cells were treated 48 hours following transfection ± 100 nmol/L JQ1. Statistical significance was measured via two-tailed, paired t tests. **F,** BRD2 density following transfection with 25 nmol/L nontargeting or BAZ2B siRNA alone and in combination with 500 nmol/L JQ1 treatment in the HCC1806 cell line. Statistical significance was measured via two-tailed, paired t tests. **G–I,** MDA-MB-231 growth curves transfected with GAPDH siRNA as a control or 25 nmol/L BRD2 siRNA (**G**), 25 nmol/L BRD3 siRNA (**H**), and 1 nmol/L BRD4 siRNA (**I**) alone and in combination with 10 μmol/L GSK2801. Error bars, ± SD, $n = 6$. P values were calculated using two-tailed t tests. **J–L,** MDA-MB-231 cells transfected with 25 nmol/L nontargeting or BRD2 siRNA alone and in combination with 25 nmol/L BAZ2A siRNA (**J**), BAZ2B siRNA (**K**), or BAZ2A + BAZ2B siRNAs (**L**). Error bars, ± SD, $n = 6$. P values were calculated using two-tailed t tests.

Displacement of BRD2 from chromatin following combination drug treatment occurs at genomic loci associated with ETS transcription factors

We sought to understand the functional consequence of BRD2 loss from chromatin in response to combination drug treatment by assessing the correlation between changes in BRD2 chromatin occupancy and gene transcription. RNA-seq revealed 1,257 genes were transcriptionally downregulated ≥two-fold in response to JQ1 in MDA-MB-231 cells. Most JQ1-responsive genes were further downregulated following the addition of GSK2801, including 235 genes downregulated two-fold or greater relative to JQ1 treatment alone (Fig. 3A). We next measured the proximity of BRD2 peaks to the 235 "combination transcriptionally-responsive" genes. Promoter and putative enhancer BRD2 peaks were defined within 5 kb or 200 kb of the gene promoter, respectively. Of the 235 combination-responsive genes, 117 had both a promoter and enhancer BRD2 peak, 7 only had measurable BRD2 at their promoter, 24 had only BRD2 enhancers, and 27 had no measurable BRD2 peaks within 200 kb of their promoter (Fig. 3B). Metagene plots of BRD2 and BRD4 at the transcription start site (tss) of combination-responsive genes showed both BET proteins were lost following JQ1 treatment, but only BRD2 was significantly lost with the addition of GSK2801 relative to JQ1 alone (Fig. 3C–F). Similar plots of enhancers showed consistent results with BRD2 density lost following combination drug treatment but not BRD4 density (Supplementary Fig. S4A and S4B). Waterfall plots measuring the fold change in BRD2 and BRD4 density following combination treatment relative to JQ1 revealed a higher resolution view of BET protein dynamics at the tss of individual responsive genes. BRD2 reads were lost at the majority of tss, whereas BRD4 displayed a larger range of responses, which did not mirror those of BRD2 (Supplementary Fig. S4C). In some cases, BRD4 was lost from the promoter of responsive genes; however, in these cases BRD2 was often lost to a greater degree. We were able to validate BAZ2A/B–dependent displacement of BRD2 at the tss of combination-responsive genes using RNAi knockdown of BAZ2A/B proteins in the presence of JQ1 (Fig. 3G and H). Similar to the global analysis (Fig. 2D and E), BAZ2B knockdown resulted in greater displacement of BRD2 from tss of responsive genes compared with BAZ2A suggesting BAZ2B is primarily responsible for BRD2 regulation at these genes. This analysis validates a BAZ2A/B–dependent loss of BRD2 at genomic loci proximal to transcriptionally responsive genes following coinhibition of BAZ2 and BET BDs.

Consensus-binding sequence analysis of BRD2 ChIP peaks using Homer software determined significant enrichment of binding motifs for class 1 ETS transcription factors and the structural protein YY1 across three TNBC cell lines: MDA-MB-231, SUM-159, and HCC1806 (Fig. 3I–K). Consistent with our results, a recent study found enrichment of ETS-binding motifs at BRD2-occupied loci in T cells as well as motifs for the structural protein CTCF (46). ETS-binding motifs were also enriched at a subset of genomic loci where BRD2 is significantly lost following combination JQ1 + GSK2801 drug treatment (Supplementary Fig. S4D and S4E). Of the 235 responsive genes, 85 contained an ETS-binding motif within 200 bp of the tss. We observed almost complete loss of BRD2 from multiple ETS-regulated genes critical for cell-cycle progression including cyclin B1, Aurora kinase A, E2F8, PLK1, LMNB1, and MAPK13 following combination drug

treatment (Fig. 3L–O; Supplementary Fig. S4F and S4G); however, BRD4 density was maintained or only slightly decreased relative to JQ1 treatment alone. These genes were transcriptionally repressed with JQ1 and further repressed with addition of GSK2801 (Supplementary Fig. S4H). GSEA of RNA-seq data from MDA-MB-231, HCC1806, and SUM-159 cells (Supplementary Data File 6) showed loss of transcriptional programs that are regulated by ETS transcription factors including c-MYC targets, core serum response, E2F targets, and G_2M checkpoint in response to combination drug treatment (Supplementary Fig. S4I). Cell-cycle analysis via propidium iodide staining revealed G_1 arrest in response to JQ1, which was enhanced with combination drug treatment (Supplementary Fig. S4J and S4K). These data indicate BRD2 regulates transcriptional programs necessary to drive cell growth, specifically those regulated by ETS transcription factors.

BRD2 is localized in the nucleolus and nucleoplasm of TNBC cells

Further inspection of GSEA revealed an enrichment of ribosome biogenesis and rRNA processing gene sets in untreated samples relative to cells treated with combination GSK2801 + JQ1 (Fig. 4A). In addition, we observed enrichment of chromatin silencing gene sets in combination-treated cells, specifically silencing at ribosomal DNA. All stages of rRNA transcription, processing, and ribosome biogenesis occur in the nucleolus. Notably, transcription of rDNA is the rate-limiting step of ribosome biogenesis and therefore serves as a rheostat of translational activity in cells. Silencing of rDNA regulates replicative senescence during aging (47, 48), and nucleolar repression is sufficient to initiate and maintain senescence in tumor cells (49, 50). We tested the localization of each BET protein to the nucleolus via immunofluorescence (Fig. 4B). BRD2 was the only BET protein that localized to both the nucleoplasm and nucleolus. BRD3 was largely present in the nucleoplasm and excluded from the nucleolus, and BRD4 was present in both the cytoplasm and nucleoplasm but also excluded from the nucleolus (Fig. 4B; Supplementary Fig. S5A and S5B). Quantification of staining confirmed BRD2 was significantly greater in the nucleolus among the BET proteins (Fig. 4C). Furthermore, BRD2 displayed greater staining density in the nucleolus when compared with its nucleoplasmic staining, which was not seen with BRD3 or BRD4 (Fig. 4D).

Dual suppression of BAZ2/BRD9 and BRD2 BDs suppresses rDNA transcription

Consistent with our immunofluorescence data, BRD2 but not BRD4 ChIP density aligned to the coding region of the rDNA repeat (Fig. 5A; Supplementary Fig. S6A and S6B). We observed modest changes in BRD2 occupancy at rDNA following single-agent treatment with either JQ1 or GSK2801; however, BRD2 was significantly lost from the rDNA coding region following combination drug treatment with greatest loss at the rDNA promoter and start of the 18S exon (Fig. 5B; Supplementary Fig. S6B). Knockdown of BRD2, but not BRD4, resulted in transcriptional loss of the 45S rRNA precursor observed by qPCR (Fig. 5C). Interestingly, rDNA is transcribed by RNA polymerase I and so these data may explain, in part, why we observed a mechanism of drug synergy between GSK2801 and JQ1 independent of P-TEFb complex regulation, which exclusively regulates pause-release of RNA polymerase II. Indeed, combination drug treatment resulted
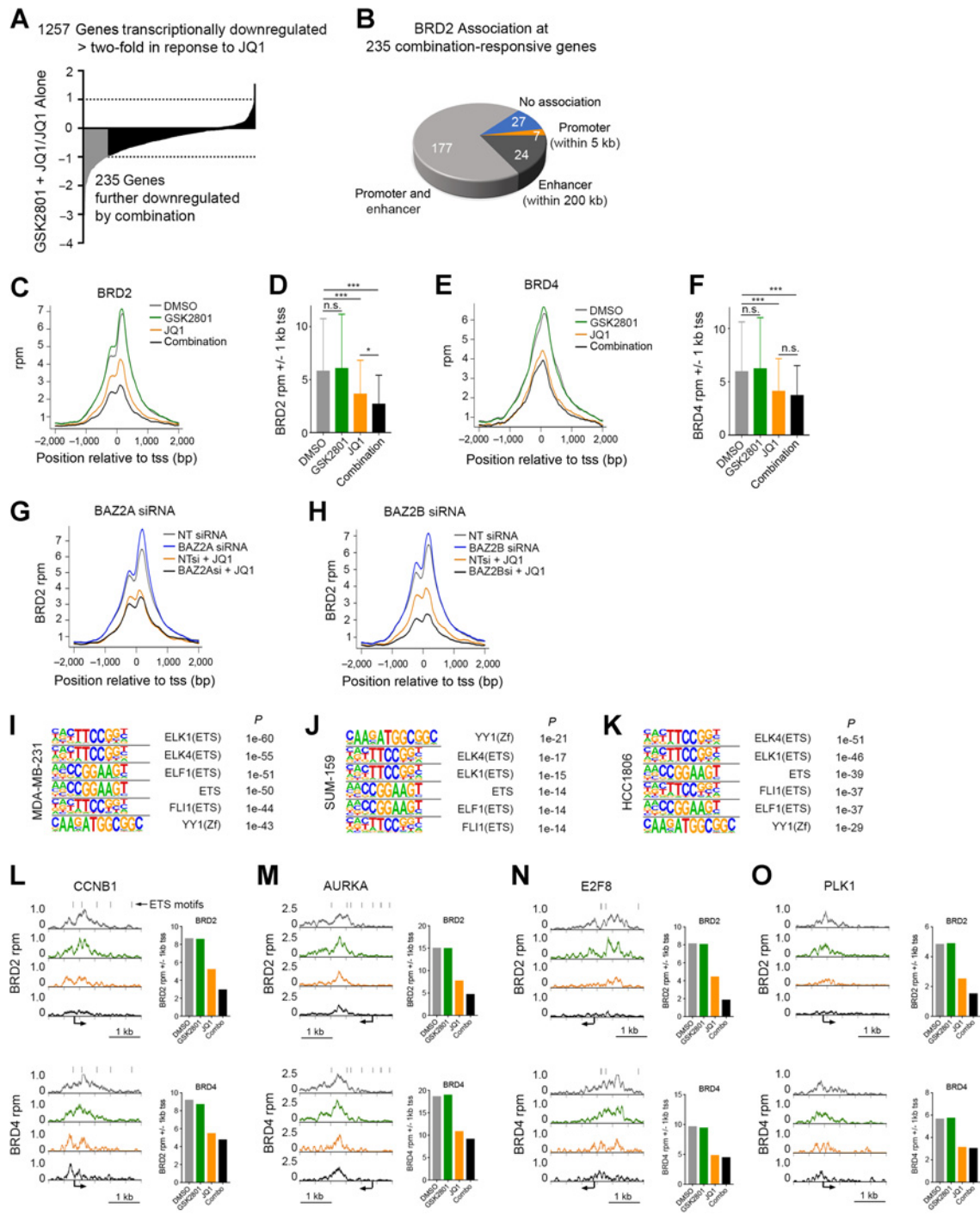
Figure 3.
BRD2 is displaced from ETS-regulated gene promoters and enhancers following combination treatment with GSK2801 and JQ1. **A,** Long tail plot of *MDA-MB-231* genes downregulated ≥two-fold following 72-hour treatment with 100 nmol/L JQ1. Values represent mRNA fold change between treatment with 10 μmol/L GSK2801 + JQ1 versus JQ1 alone. Genes highlighted in gray were downregulated ≥two-fold in combination-treated cells relative to JQ1 alone. **B,** Association of BRD2 peaks with "combination-responsive" genes in DMSO treated MDA-MB-231 cells. **C–F,** Metagene plots of BRD2 (**C**) and BRD4 (**E**) density at tss of "combination-responsive" genes. MDA-MB-231 cells were treated 48 hours with DMSO, 10 μmol/L GSK2801, 100 nmol/L JQ1, or the combination. Bar plots, total read counts of BRD2 (**D**) or BRD4 (**F**) ± 1 kb of the tss. *P* values were calculated via two-tailed, paired *t* tests (**G–H**) Metagene plots of BRD2 density at tss of "combination-responsive" genes following transfection with BAZ2A (**G**) or BAZ2B (**H**) siRNA. MDA-MB-231 cells were treated 48 hours with and without 100 nmol/L JQ1 following transfection. **I–K,** Motif analysis of BRD2 binding in DMSO-treated samples of MDA-MB-231 (**I**), SUM-159 (**J**), and HCC1806 (**K**) cell lines. **L–O,** BRD2 and BRD4 ChIP-seq density tracks following 48-hour treatment with DMSO, 10 μmol/L GSK2801, 100 nmol/L JQ1, or the combination in MDA-MB-231 cells. Black bars, ETS-binding motifs. Bar plots, total read counts of BRD2 or BRD4 ± 1 kb of the tss.
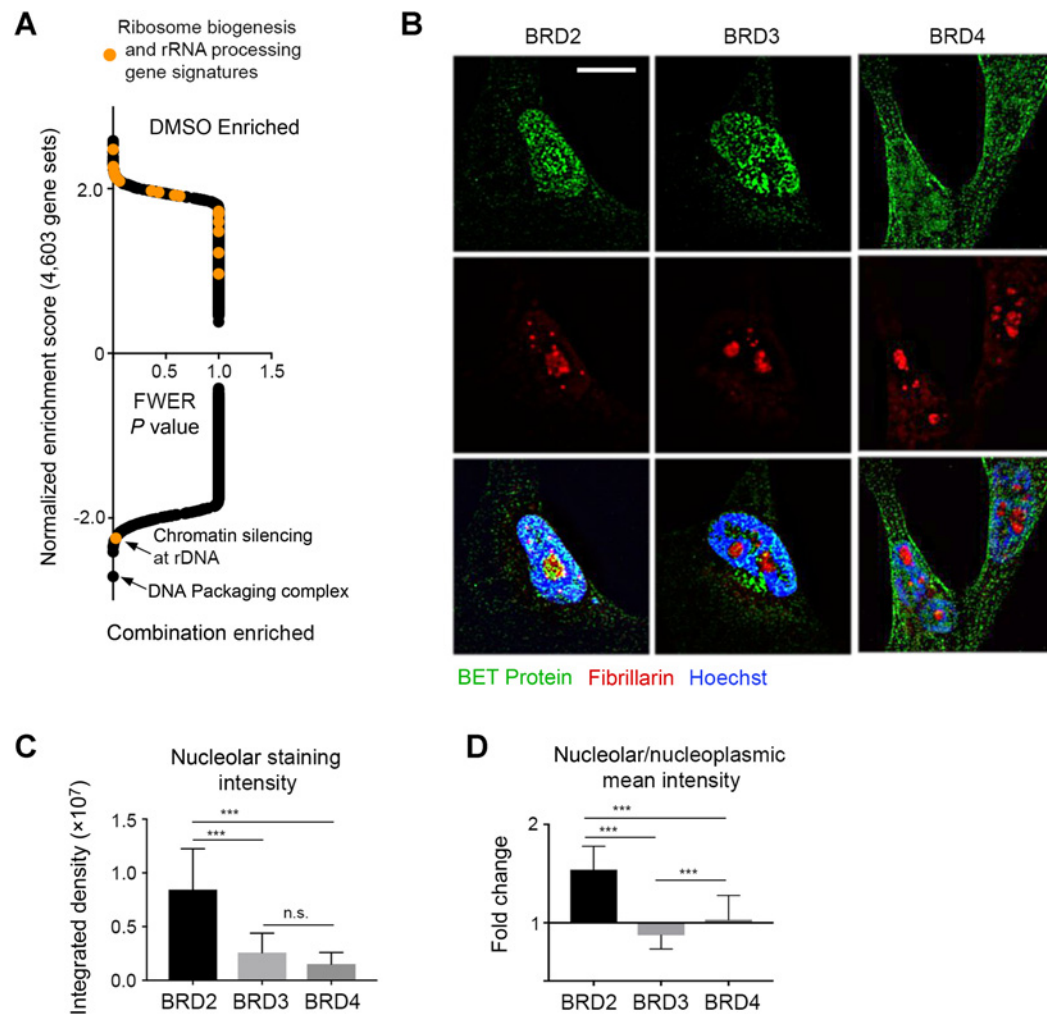
Figure 4.
BRD2 is the only BET protein localized to the nucleolus. **A,** GSEA of MDA-MB-231, HCC1806, and SUM-159 RNA-seq datasets treated 72 hours with 10 µmol/L GSK2801 and 100 nmol/L JQ1 (MDA-MB-231 and SUM-159) or 500 nmol/L JQ1 (HCC1806). Orange values, ribosome biogenesis or rRNA processing gene signatures. Positive enrichment scores, gene sets enriched in DMSO. Negative enrichment scores, gene sets enriched in GSK2801 + JQ1–treated samples. **B,** Immunofluorescent staining of BET proteins with fibrillarin (nucleolar marker) and Hoechst (nuclear marker). **C** and **D,** Quantification of nucleolar versus nucleoplasmic staining intensity of BET proteins. A one-way ANOVA was conducted to compare intensity of BET protein staining, $P < 2e\text{-}16$ for **C** and **D**. *Post hoc* comparisons were made using the Tukey HSD test.

in loss of the 45S rRNA specifically in combination-treated samples across multiple cell lines (Fig. 5D–F). We performed S^{35} methionine labeling experiments to quantify global translation in response to drug in MDA-MB-231 cells. Although these results largely mirrored cell growth, we saw marked loss of S^{35} methionine incorporation following combination drug treatment (Fig. 5G). These data support a novel role of BRD2 in positively regulating rRNA transcription and suggest loss of rRNA, and subsequent translation, during combination drug treatment contributes to synergistic growth inhibition.

BAZ2A is present in the nucleolus and nucleoplasm and is coregulated with BET BD proteins

Because of the lack of commercial antibodies with selective specificity for BAZ proteins needed for ChIP, we used CRISPR to engineer a C-terminal in-frame V5 epitope tag in the *BAZ2A* gene

in MDA-MB-231 cells (Supplementary Fig. S7A and S7B). The presence of multiple alternative tss and lack of C-terminal sequence required for guide RNA design prohibited us from successfully tagging BAZ2B. Immunoblotting confirmed BAZ2A-V5 was expressed at similar levels as BAZ2A protein in parental cells (Fig. 6A). ChIP-seq using a V5 antibody revealed BAZ2A-V5 bound the coding region of rDNA in a similar pattern as seen with BRD2 but not BRD4 or BRD9 (Fig. 6B). The presence of BAZ2A-V5 in the nucleolus is consistent with the published function of BAZ2A (TIP5) as a member of the nucleolar remodeling complex. These findings are consistent with BAZ2A being associated with transcriptional complexes containing BRD2 within the nucleolus.

Immunofluorescent imaging confirmed BAZ2A-V5 staining in the nucleolus with significantly stronger staining density of BAZ2A-V5 in the nucleoplasm (Fig. 6C and D). Quantification
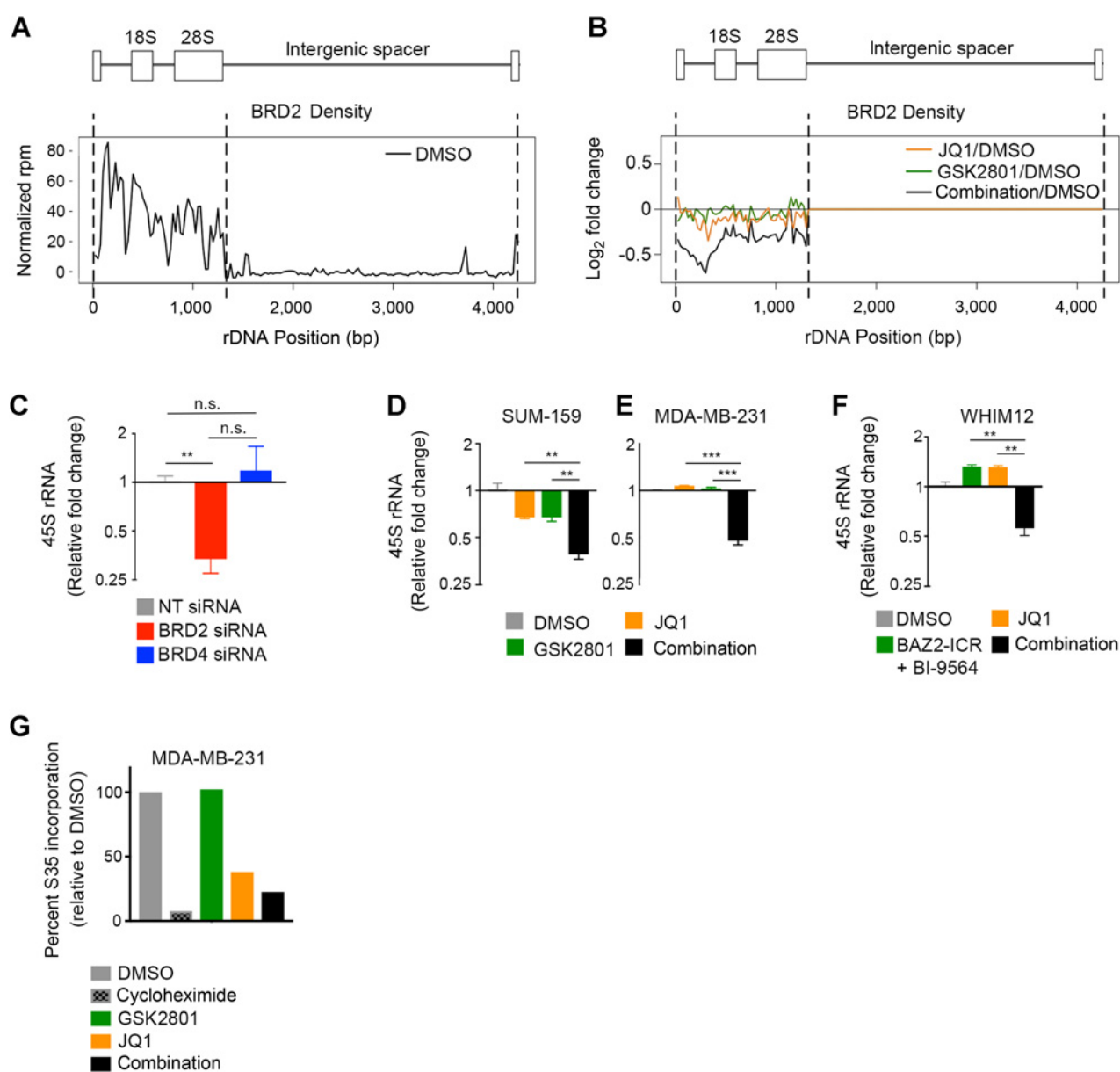
Figure 5.
Displacement of BRD2 from the rDNA repeat coincides with transcriptional repression of rRNA. **A,** Alignment of BRD2 ChIP-seq reads to the rDNA repeat in MDA-MB-231 cells. **B,** Response of BRD2 density on rDNA in response to 48-hour treatment with DMSO, 10 μmol/L GSK2801, 100 nmol/L JQ1, or the combination in MDA-MB-231 cells. **C,** qPCR measuring 45S rRNA following 96-hour transfection with nontargeting (NT), BRD2, or BRD4 siRNA in MDA-MB-231 cells. Error bars, SD, $n = 3$. P values were calculated using two-tailed t tests. **D** and **E,** qPCR measuring 45S rRNA in SUM-159 (**D**) and MDA-MB-231 (**E**) cells following 96-hour treatment with DMSO, 10 μmol/L GSK2801, 100 nmol/L JQ1, or the combination. Error bars, SD, $n = 3$. P values were calculated using two-tailed t tests. **F,** qPCR measuring 45S rRNA in the WHIM12 cell line following 96-hour treatment with 500 nmol/L JQ1 $\pm$ 10 μmol/L BAZ2-ICR and 300 nmol/L BI-9564. Error bars, SD, $n = 3$. P values were calculated using two-tailed t tests. **G,** S^{35} labeling of protein production in MDA-MB-231 cells following 72-hour treatment with 10 μmol/L GSK2801, 100 nmol/L JQ1, or the combination. A total of 100 μg/mL cycloheximide treatment was included as a positive control.

of staining revealed that, on average, only 10% of total BAZ2A-V5 staining in the nucleus was restricted to the nucleolus (Fig. 6E).

Quantification of global BAZ2A-V5 chromatin occupancy revealed a significant loss of BAZ2A-V5 from chromatin following inhibition of its BD by GSK2801 (Fig. 6F). We also observed significant global displacement of BAZ2A following treatment with the BETi JQ1, suggesting BAZ2A is coregulated with BET BD proteins such as BRD2 on chromatin.

Combination treatment with BAZ2/BRD9 and BET BD inhibitors induces senescence and apoptosis

To further characterize the cellular phenotype in response to combination drug treatment, we performed beta-galactosidase (β-gal) staining of TNBC cell lines grown in 2D cultures treated with drug for 96 hours. Combination drug treatment resulted in a higher percentage of β-gal–positive cells relative to JQ1 alone (Fig. 7A–D). Again, treatment with a selective BAZ2A/B BD
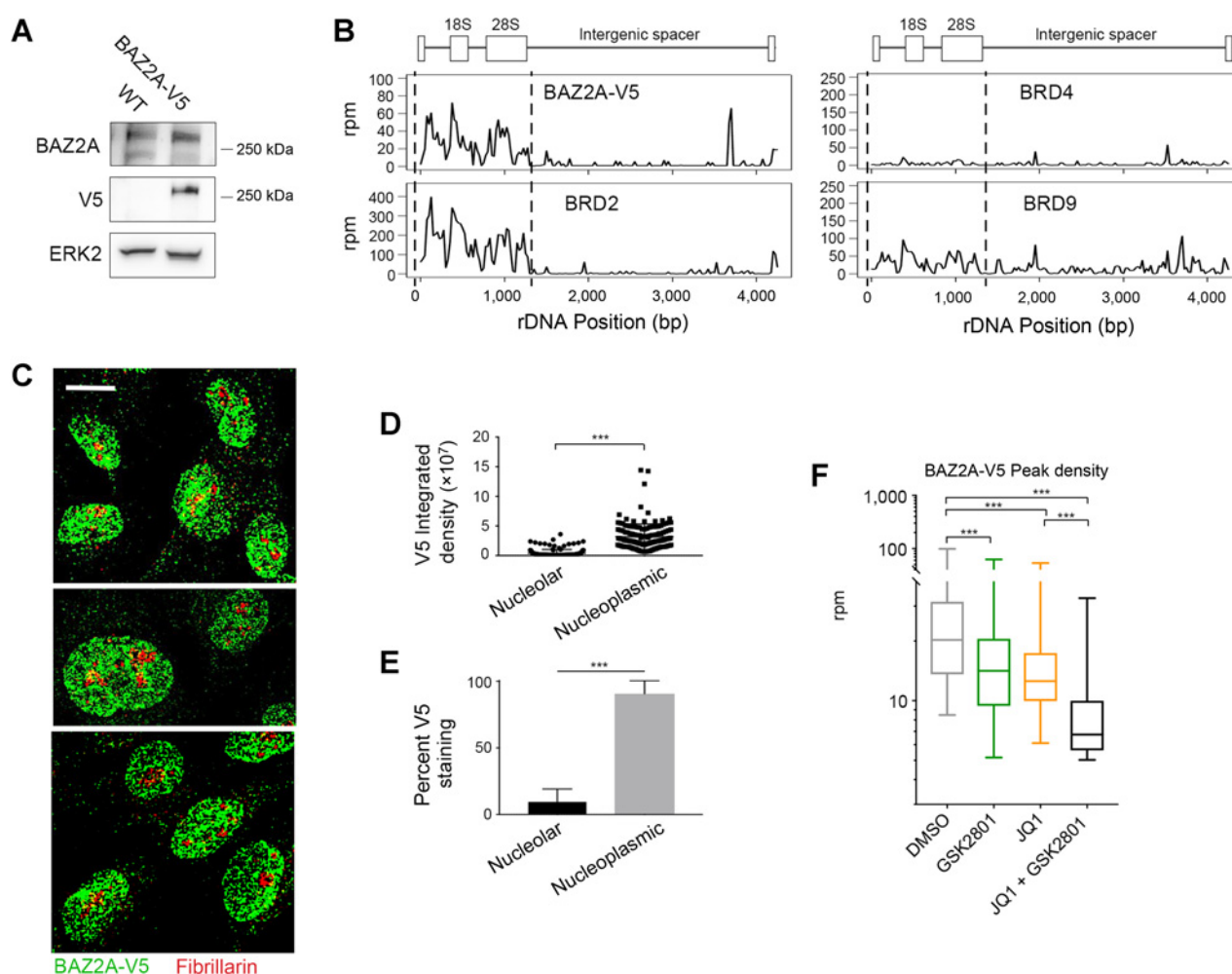
Figure 6.
BAZ2A is coregulated with BRD2 in the nucleolus and nucleoplasm. **A,** Western blot analysis of MDA-MB-231 cell lysate expressing wild-type BAZ2A versus BAZ2A-V5. **B,** Alignment of BAZ2A-V5, BRD2, BRD4, and BRD9 ChIP-seq reads to the rDNA repeat in MDA-MB-231 cells. **C,** Representative images of immunofluorescent staining of BAZ2A-V5 with fibrillarin (nucleolar marker). **D** and **E,** Quantification of nucleolar versus nucleoplasmic staining intensity of V5 in approximately 200 individual cells. **F,** Levels of BAZ2A-V5 union peak density following 48-hour treatment with 100 nmol/L JQ1, 10 μmol/L GSK2801, or the combination in MDA-MB-231 cells.

inhibitor, BAZ-ICR, induced a partial response and it was not until the addition of the BRD9 inhibitor, BI-9564, that we saw a similar percentage of β-gal–positive cells compared with GSK2801. This confirms that although BAZ2A/B inhibition is contributing to synergistic growth inhibition, the effect of GSK2801 on BRD9 also contributes to drug synergy. Positive β-gal staining suggests that cells are entering a senescent state following combination drug treatment. We looked at which drivers of senescence signaling were responsible for the phenotype. All cell lines screened contain *TP53* mutations common to TNBC, and most cell lines also contain deletion or transcriptional silencing of *CDKN2A* (p16; Supplementary Fig. S8A). This left *CDKN1A* (p21) and *RB1*, the retinoblastoma tumor suppressor as candidate regulators of senescence. RNA-seq data showed induction of p21 transcript levels following a dose of JQ1 that induces modest β-gal staining (Supplementary Fig. S8B). Western blots in multiple cell lines confirmed induction of p21 protein levels and decrease in phospho-Rb in combination-treated samples

(Fig. 7E–G; Supplementary Fig. S8C and S8D). While knockdown of p21 via RNAi was able to rescue JQ1 growth inhibition, it only partially rescued growth inhibition of combination drug–treated cells (Fig. 7H). These data suggest induction of p21 only partially regulates the senescent state of cells treated with JQ1 and GSK2801. It is therefore likely treatment with BAZ2A/B/BRD9i and BETi results in senescence via multiple mechanisms. First, inhibition of cell-cycle gene transcription results in G_1 arrest and induction of p21. Secondly, this growth arrest is likely enhanced by nucleolar suppression and translational silencing following loss of BRD2 from the rDNA promoter.

GSK2801 has poor pharmacokinetics in mice combined with a relatively high IC_{50} for the BAZ2/BRD9 BDs (41), so we tested combination drug treatment in 3D-spheroid models (Fig. 7I–L; Supplementary Fig. S8E and S8F). Breast cancer cells expressing RFP were cocultured with RMFs expressing GFP. We observed a dramatic reduction in breast tumor cell fluorescence following 10-day combination treatment compared with either single agent
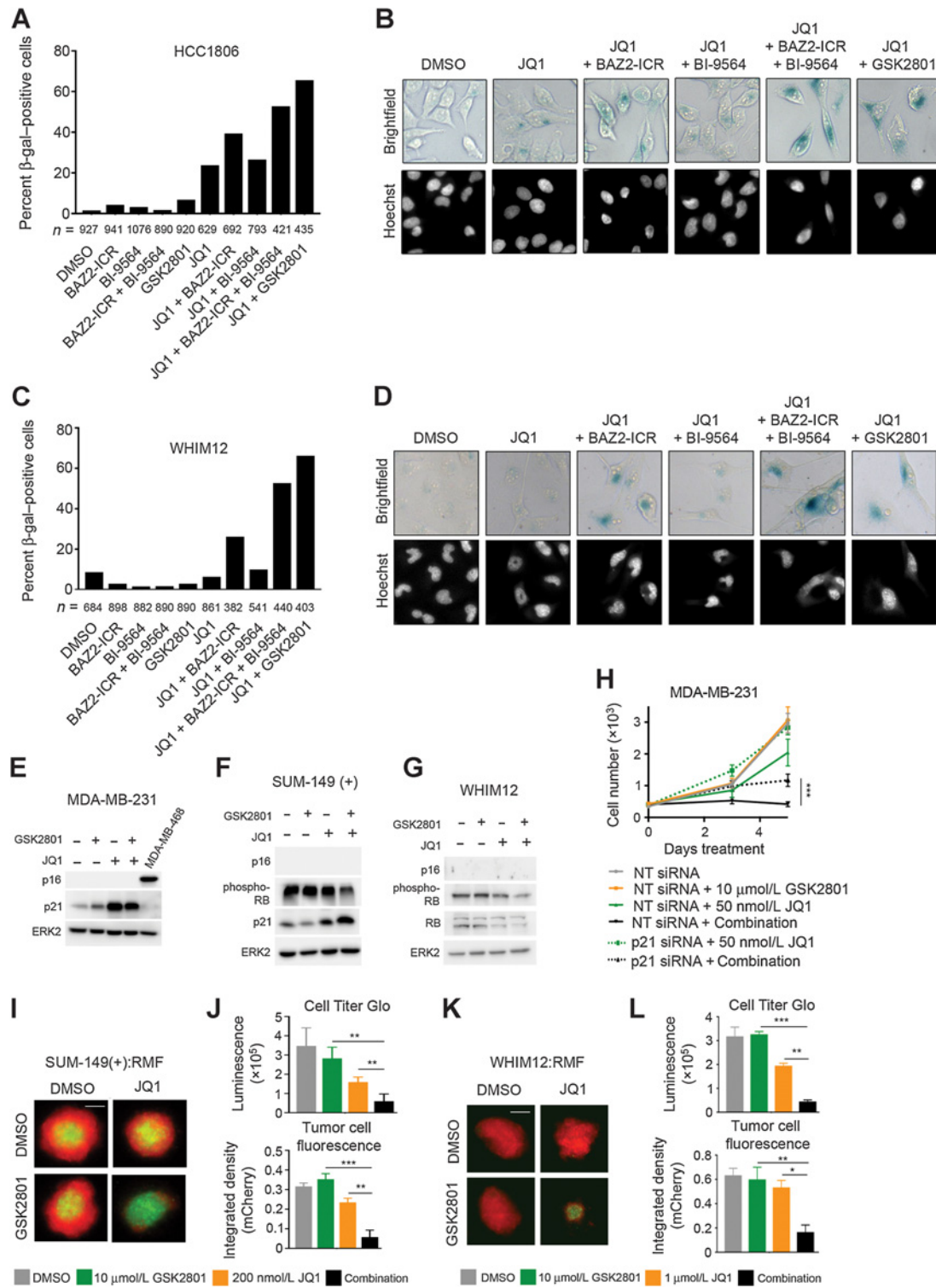
Figure 7.
Combined GSK2801 and JQ1 treatment induces senescence and apoptosis in TNBC cell lines. **A–D,** Senescence-associated β-gal staining in HCC1806 (**A–B**) and WHIM12 (**C–D**) cell lines following 96-hour drug treatment. Cells were dosed with 10 μmol/L GSK2801, 10 μmol/L BAZ2-ICR, 1 μmol/L BI-9564, and either 300 nmol/L JQ1 (HCC1806) or 500 nmol/L JQ1 (WHIM12). **E–G,** Western blots of MDA-MB-231 (**E**), SUM-149(+) (**F**), and WHIM12 (**G**) cell lysates following 72-hour treatment with 10 μmol/L GSK2801 and either 100 nmol/L JQ1 (MDA-MB-231), 300 nmol/L JQ1 (SUM-149(+)), or 500 nmol/L JQ1 (WHIM12). **H,** MDA-MB-231 cells transfected with 25 nmol/L nontargeting (NT) or p21 siRNA alone and in combination with 10 μmol/L GSK2801 and 50 nmol/L JQ1. Error bars, ± SD, $n = 6$. **I–L,** 3D spheroids with SUM-149(+) and WHIM12 cell lines cocultured with RMFs treated 10 days with GSK2801 and JQ1. Tumor cell fluorescence was measured at endpoint and cell viability was measured with CellTiter-Glo 3D reagent, Error bars, ± SD, $n = 3$. P values were calculated using two-tailed t tests.

alone in SUM-149(+) and WHIM12 cell lines (Fig. 7I–L). This was consistent with ATP measurements using CellTiter-Glo 3D reagent, which showed diminished cell viability in the combination-treated spheroids. There was no reduction in fluorescence from the normal breast fibroblast population following drug treatment, indicating a selective loss of tumor cell viability (Supplementary Fig. S8E and S8F). Monoculture spheroids established using only SUM-149(+) tumor cells displayed cleaved caspase-3 and cleaved PARP following 36-hour treatment with combination GSK2801 + 100 nmol/L or 300 nmol/L JQ1 (Supplementary Fig. S8G). Apoptosis was only present in spheroids treated with both drugs and not with either JQ1 or GSK2801 alone. These results were consistent with CellTiter-Glo measurements, which showed dose-dependent reduction in cell viability with increasing doses of JQ1 in combination with GSK2801 (Supplementary Fig. S8H). These data highlight coinhibition of BAZ2/BRD9 and BET BDs as an effective strategy to induce apoptosis in TNBC.

Discussion

Ten BET BD inhibitors are currently in different phases of clinical trials for multiple tumor types including breast cancer (ClinicalTrials.gov). Despite some dose-dependent toxicity such as thrombocytopenia, the tolerability of different BETi in patients suggests that synergistic combination therapies may be practical. We previously showed the relevance of synergistic combination therapies with BETi in both HER2+ and TNBC preclinical models, demonstrating that BETi effectively blocks epigenetic transcriptional reprogramming making targeted kinase inhibitors, lapatinib and trametinib, more durable in their inhibition of tumor growth *in vitro* and *in vivo* (6, 7). Our BETi screens identified inhibitors of MEK1/2-ERK1/2, CDK9, CBP/p300, and Aurora kinase as synergistic drug combinations with multiple TNBC cell lines. Trametinib and selumetinib are FDA-approved MEK1/2 inhibitors and there are multiple Aurora kinase inhibitors currently in all phases of clinical trials, alone and in different combinations with chemotherapy and targeted therapeutics (ClinicalTrials.gov). Therefore, BETi combination trials with MEK1/2 or Aurora kinase inhibitors could be initiated quickly because of the substantial knowledge of pharmacology and tolerability of each in patient trials.

The BDs of BAZ2/BRD9 were identified as novel targets for synergy with BETi to produce antiproliferative responses for multiple TNBC cell lines. The synergy seen with GSK2801 was regulated by a different mechanism than inhibitors targeting CBP/p300 and CDK9 of the P-TEFb transcriptional regulatory complex that is associated with BRD4. Instead, the uniqueness of this combination treatment is selective enhancement of BRD2 chromatin release in response to inhibition of BAZ2/BRD9 BDs.

While our data support a mechanism of synergy by which BRD9 modulates cell growth through regulation of *MYC* expression, it is possible BRD9 is involved in regulation of BRD2 or BAZ2 proteins. ChIP data show overlap between BRD2 and BRD9 peaks at regions where BRD2 is responsive to drug treatment. However, we do not observe the same displacement of BRD9 from chromatin following combination drug treatment as we see with BRD2. BRD9 is released from chromatin in response to JQ1 treatment alone, even though JQ1 does not bind the BRD9 BD, demonstrating the complexity of the BD-encoded proteins and their interaction with chromatin.

Genes regulated by ETS transcription factors and the 45S rDNA promoter are selectively targeted by GSK2801 in combination with JQ1 for loss of BRD2, as defined by ChIP assay. Targeting of ETS-regulated genes and ribosomal RNA transcription using GSK2801 + JQ1 gave a strong antiproliferative response combined with the induction of proapoptotic caspase-3 activity and PARP cleavage in 3D cultures. To date, the most tractable inhibitor of the BAZ2A/B BD is GSK2801, which also binds the BRD9 BD. Inhibition of the BRD9 BD clearly contributed to the antiproliferative action of the JQ1 + GSK2801 combination treatment. Use of this tool compound enabled us to establish inhibition of BAZ2/BRD9 BDs as an effective means to block BRD2-driven transcription in combination with BETi in TNBC 2D cultures and 3D-spheroid models. Why senescence is observed in 2D cultures and apoptosis observed in 3D cultures is unclear, but most likely is related to the adherence and cell interaction differences in the two models.

TNBCs do not contain significant mutations or copy-number alterations in BAZ2A, BAZ2B, or BRD9. Our study is the first to highlight BAZ2A/B and BRD9 as targetable vulnerabilities in TNBC in the context of BETi. Noncanonical functions of BAZ2A have been previously characterized in driving cancer phenotypes. Overexpression of BAZ2A in prostate cancer predicts disease recurrence and, in this context, BAZ2A was shown to interact with EZH2 and modulate expression of protein-coding genes in the nucleoplasm (51). BAZ2A also interacts with TCF7L2 to drive β-catenin signaling and promote growth in hepatocellular carcinoma (52). There is less direct evidence for BAZ2B's involvement in cancer but hypomethylation of the *BAZ2B* gene is associated with poor outcome in acute lymphoblastic leukemia (53), suggesting it may play a functional role in driving tumor growth and progression. The distinct functional roles of BAZ2A in cancer suggest inhibition of its BD may result in tumor-specific toxicity. Together our findings present coinhibition of BAZ2A/B and BRD9 BDs in combination with BET protein BD inhibition as an effective strategy to block nucleoplasmic and nucleolar BRD2-regulated transcription for growth arrest, and induction of apoptosis of TNBC.

References

1. Delmore JE, Issa GC, Lemieux ME, Rahl PB, Shi J, Jacobs HM, et al. BET bromodomain inhibition as a therapeutic strategy to target c-Myc. Cell 2011;146:904–17.
2. Ott CJ, Kopp N, Bird L, Paranal RM, Qi J, Bowman T, et al. BET bromo-domain inhibition targets both c-Myc and IL7R in high-risk acute lymphoblastic leukemia. Blood 2012;120:2843–52.
3. Zuber J, Shi J, Wang E, Rappaport AR, Herrmann H, Sison EA, et al. RNAi screen identifies Brd4 as a therapeutic target in acute myeloid leukaemia. Nature 2011;478:524–8.
4. Hargreaves DC, Horng T, Medzhitov R. Control of inducible gene expression by signal-dependent transcriptional elongation. Cell 2009;138:129–45.
5. Itzen F, Greifenberg AK, Bösken CA, Geyer M. Brd4 activates P-TEFb for RNA polymerase II CTD phosphorylation. Nucleic Acids Res 2014;42:7577–90.
6. Zawistowski JS, Bevill SM, Goulet DR, Stuhlmiller TJ, Beltran AS, Olivares-Quintero JF, et al. Enhancer remodeling during adaptive bypass to MEK inhibition is attenuated by pharmacologic targeting of the P-TEFb complex. Cancer Discov 2017;7:302–21.
7. Stuhlmiller TJ, Miller SM, Zawistowski JS, Nakamura K, Beltran AS, Duncan JS, et al. Inhibition of lapatinib-induced kinome reprogramming in ERBB2-positive breast cancer by targeting BET family bromo-domains. Cell Rep 2015;11:390–404.
8. Stratikopoulos EE, Dendy M, Szabolcs M, Khaykin AJ, Lefebvre C, Zhou M-M, et al. Kinase and BET inhibitors together clamp inhibition of PI3K signaling and overcome resistance to therapy. Cancer Cell 2015;27:837–51.
9. De Raedt T, Beert E, Pasmant E, Luscan A, Brems H, Ortonne N, et al. PRC2 loss amplifies Ras-driven transcription and confers sensitivity to BRD4-based therapies. Nature 2014;514:247–51.
10. Perez-Pena J, Serrano-Heras G, Montero JC, Corrales-Sanchez V, Pandiella A, Ocana A. In silico analysis guides selection of BET inhibitors for triple-negative breast cancer treatment. Mol Cancer Ther 2016;15:1823–33.
11. Sahni JM, Gayle SS, Bonk KL, Vite LC, Yori JL, Webb B, et al. Bromodomain and extraterminal protein inhibition blocks growth of triple-negative breast cancers through the suppression of Aurora kinases. J Biol Chem 2016;291:23756–68.
12. Shu S, Lin CY, He HH, Witwicki RM, Tabassum DP, Roberts JM, et al. Response and resistance to BET bromodomain inhibitors in triple-negative breast cancer. Nature 2016;529:413–7.
13. Schneider BP, Winer EP, Foulkes WD, Garber J, Perou CM, Richardson A, et al. Triple-negative breast cancer: risk factors to potential targets. Clin Cancer Res 2008;14:8010–8.
14. Sorlie T, Perou CM, Tibshirani R, Aas T, Geisler S, Johnsen H, et al. Gene expression patterns of breast carcinomas distinguish tumor subclasses with clinical implications. Proc Natl Acad Sci U S A 2001;98:10869–74.
15. Erdel F, Rippe K. Chromatin remodelling in mammalian cells by ISWI-type complexes - where, when and why?: ISWI chromatin remodellers in mammalian cells. FEBS J 2011;278:3608–18.
16. Strohner R. NoRC–a novel member of mammalian ISWI-containing chromatin remodeling machines. EMBO J 2001;20:4892–900.
17. Guetg C, Lienemann P, Sirri V, Grummt I, Hernandez-Verdun D, Hottiger MO, et al. The NoRC complex mediates the heterochromatin formation and stability of silent rRNA genes and centromeric repeats. EMBO J 2010; 29:2135–46.
18. Postepska-Igielska A, Krunic D, Schmitt N, Greulich-Bode KM, Boukamp P, Grummt I. The chromatin remodelling complex NoRC safeguards genome stability by heterochromatin formation at telomeres and centromeres. EMBO Rep 2013;14:704–10.
19. Oppikofer M, Bai T, Gan Y, Haley B, Liu P, Sandoval W, et al. Expansion of the ISWI chromatin remodeler family with new active complexes. EMBO Rep 2017;18:1697–706.
20. Minzel W, Venkatachalam A, Fink A, Hung E, Brachya G, Burstain I, et al. Small molecules co-targeting CKIα and the transcriptional kinases CDK7/9 control AML in preclinical models. Cell 2018;175:171–85.
21. Hohmann AF, Martin LJ, Minder JL, Roe JS, Shi J, Steurer S, et al. Sensitivity and engineered resistance of myeloid leukemia cells to BRD9 inhibition. Nat Chem Biol 2016;12:672–9.
22. Ianevski A, He L, Aittokallio T, Tang J. SynergyFinder: a web application for analyzing drug combination dose-response matrix data. Bioinformatics 2017;33:2413–5.
23. Wang K, Singh D, Zeng Z, Coleman SJ, Huang Y, Savich GL, et al. MapSplice: accurate mapping of RNA-seq reads for splice junction discovery. Nucleic Acids Res 2010;38:e178.
24. Li H, Handsaker B, Wysoker A, Fennell T, Ruan J, Homer N, et al. The Sequence Alignment/Map format and SAMtools. Bioinformatics 2009;25:2078–9.
25. Li B, Dewey CN. RSEM: accurate transcript quantification from RNA-Seq data with or without a reference genome. BMC Bioinformatics 2011;12:323.
26. Dobin A, Davis CA, Schlesinger F, Drenkow J, Zaleski C, Jha S, et al. STAR: ultrafast universal RNA-seq aligner. Bioinformatics 2013;29:15–21.
27. Patro R, Duggal G, Love MI, Irizarry RA, Kingsford C. Salmon provides fast and bias-aware quantification of transcript expression. Nat Methods 2017; 14:417–9.
28. Durinck S, Moreau Y, Kasprzyk A, Davis S, De Moor B, Brazma A, et al. BioMart and bioconductor: a powerful link between biological databases and microarray data analysis. Bioinformatics 2005;21:3439–40.
29. Langmead B, Trapnell C, Pop M, Salzberg SL. Ultrafast and memory-efficient alignment of short DNA sequences to the human genome. Genome Biol 2009;10:R25.
30. Pruitt KD, Tatusova T, Maglott DR. NCBI reference sequences (RefSeq): a curated non-redundant sequence database of genomes, transcripts and proteins. Nucleic Acids Res 2007 Jan;35:D61–65.
31. Zhang Y, Liu T, Meyer CA, Eeckhoute J, Johnson DS, Bernstein BE, et al. Model-based analysis of ChIP-Seq (MACS). Genome Biol 2008;9:R137.
32. Ashoor H, Hérault A, Kamoun A, Radvanyi F, Bajic VB, Barillot E, et al. HMCan: a method for detecting chromatin modifications in cancer samples using ChIP-seq data. Bioinformatics 2013;29:2979–86.
33. Lovén J, Hoke HA, Lin CY, Lau A, Orlando DA, Vakoc CR, et al. Selective inhibition of tumor oncogenes by disruption of super-enhancers. Cell 2013;153:320–34.
34. Heinz S, Benner C, Spann N, Bertolino E, Lin YC, Laslo P, et al. Simple combinations of lineage-determining transcription factors prime cis-regulatory elements required for macrophage and B cell identities. Mol Cell 2010;38:576–89.
35. Saldanha AJ. Java Treeview–extensible visualization of microarray data. Bioinformatics 2004;20:3246–8.
36. Koboldt DC, Fulton RS, McLellan MD, Schmidt H, Kalicki-Veizer J, McMichael JF, et al. Comprehensive molecular portraits of human breast tumours. Nature 2012;490:61–70.
37. Prat A, Parker JS, Karginova O, Fan C, Livasy C, Herschkowitz JI, et al. Phenotypic and molecular characterization of the claudin-low intrinsic subtype of breast cancer. Breast Cancer Res 2010;12:R68.
38. Yadav B, Wennerberg K, Aittokallio T, Tang J. Searching for drug synergy in complex dose-response landscapes using an interaction potency model. Comput Struct Biotechnol J 2015;13:504–13.
39. Boi M, Gaudio E, Bonetti P, Kwee I, Bernasconi E, Tarantelli C, et al. The BET bromodomain inhibitor OTX015 affects pathogenetic pathways in

preclinical B-cell tumor models and synergizes with targeted drugs. Clin Cancer Res 2015;21:1628–38.

40. Jones MH, Hamana N, Nezu JI, Shimane M. A novel family of bromodomain genes. Genomics 2000;63:40–5.

41. Chen P, Chaikuad A, Bamborough P, Bantscheff M, Bountra C, Chung C, et al. Discovery and characterization of GSK2801, a selective chemical probe for the bromodomains BAZ2A and BAZ2B. J Med Chem 2016;59: 1410–24.

42. Drouin L, McGrath S, Vidler LR, Chaikuad A, Monteiro O, Tallant C, et al. Structure enabled design of BAZ2-ICR, a chemical probe targeting the bromodomains of BAZ2A and BAZ2B. J Med Chem 2015;58:2553–9.

43. Ciceri P, Müller S, O'Mahony A, Fedorov O, Filippakopoulos P, Hunt JP, et al. Dual kinase-bromodomain inhibitors for rationally designed polypharmacology. Nat Chem Biol 2014;10:305–12.

44. Dittmann A, Werner T, Chung CW, Savitski MM, Fälth Savitski M, Grandi P, et al. The commonly used PI3-kinase probe LY294002 is an inhibitor of BET bromodomains. ACS Chem Biol 2014;9:495–502.

45. Ember SW, Lambert QT, Berndt N, Gunawan S, Ayaz M, Tauro M, et al. Potent dual BET bromodomain-kinase inhibitors as value-added multitargeted chemical probes and cancer therapeutics. Mol Cancer Ther 2017; 16:1054–67.

46. Cheung KL, Zhang F, Jaganathan A, Sharma R, Zhang Q, Konuma T, et al. Distinct roles of Brd2 and Brd4 in potentiating the transcriptional program for Th17 cell differentiation. Mol Cell 2017;65:1068–80.

47. Comai L. The nucleolus: a paradigm for cell proliferation and aging. Braz J Med Biol Res 1999;32:1473–8.

48. Guarente L. Link between aging and the nucleolus. Genes Dev 1997;11: 2449–55.

49. Nishimura K, Kumazawa T, Kuroda T, Katagiri N, Tsuchiya M, Goto N, et al. Perturbation of ribosome biogenesis drives cells into senescence through 5S RNP-mediated p53 activation. Cell Rep 2015;10:1310–23.

50. Yang L, Song T, Chen L, Soliman H, Chen J. Nucleolar repression facilitates initiation and maintenance of senescence. Cell Cycle 2015; 14:3613–23.

51. Gu L, Frommel SC, Oakes CC, Simon R, Grupp K, Gerig CY, et al. BAZ2A (TIP5) is involved in epigenetic alterations in prostate cancer and its overexpression predicts disease recurrence. Nat Genet 2015;47:22–30.

52. Li C, Wu W, Ding H, Li Q, Xie K. The transcription factor 7 like 2-binding protein TIP5 activates β-catenin/transcription factor signaling in hepatocellular carcinoma. Mol Med Rep 2018;17:7645–51.

53. Navarrete-Meneses MDP, Pérez-Vera P. Epigenetic alterations in acute lymphoblastic leukemia. Bol Méd Hosp Infant Mex 2017;74:243–64.